A femtotesla equivalent magnetic noise magnetoelectric sensor

Lizhi Hu,[1,3] Jie Jiao,[2,3] Ze Fang,[1] Shichao Hao,[1] Shuhao Wang,[1] Lisha Liu,[1] and Yaojin Wang[1,*]
*Correspondence: yjwang@njust.edu.cn
Received: September 4, 2025; Accepted: February 7, 2026; Published Online: February 7, 2026; https://doi.org/10.59717/j.xinn-mater.2026.100205

GRAPHICAL ABSTRACT

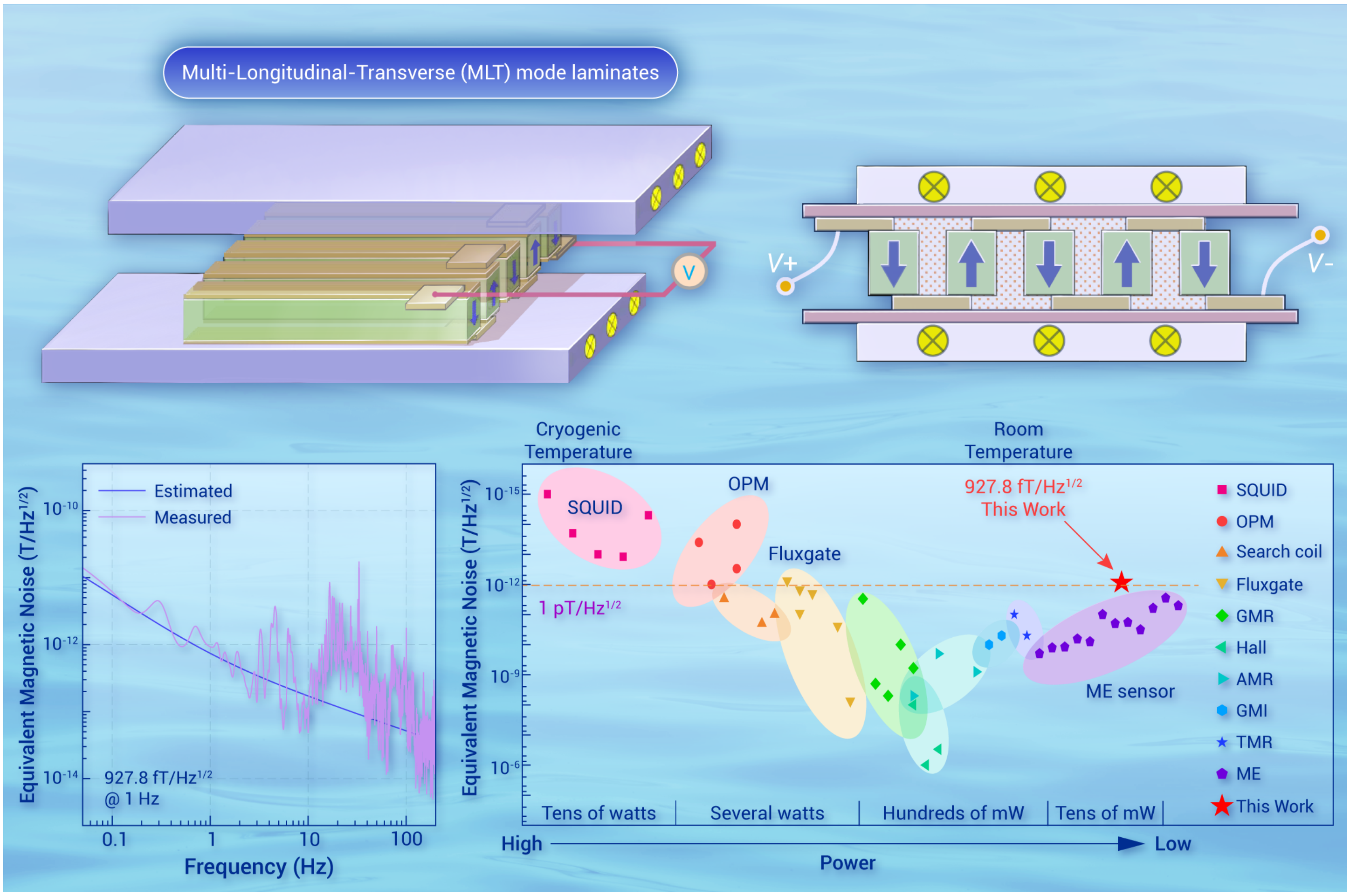

PUBLIC SUMMARY

- We developed a magnetoelectric sensor achieving the equivalent magnetic noise of 927.8 $fT/Hz^{1/2}$ at 1 Hz.
- A multi-parameter synergistic optimization is proposed to guide the sensor design.
- The multi-longitudinal-transverse mode laminates is utilized to significantly suppress the intrinsic noise.

A femtotesla equivalent magnetic noise magnetoelectric sensor

Lizhi Hu,[1,3] Jie Jiao,[2,3] Ze Fang,[1] Shichao Hao,[1] Shuhao Wang,[1] Lisha Liu,[1] and Yaojin Wang[1,*]
[1]School of Materials Science and Engineering, Nanjing University of Science and Technology, Nanjing 210094, China
[2]State Key Laboratory of Functional Crystals and Devices, Shanghai Institute of Ceramics, Chinese Academy of Sciences, Shanghai 201899, China
[3]These authors contributed equally
*Correspondence: yjwang@njust.edu.cn

Received: September 4, 2025; Accepted: February 7, 2026; Published Online: February 7, 2026; https://doi.org/10.59717/j.xinn-mater.2026.100205

Citation: Hu L., Jiao J., Fang Z., et al. (2026). A femtotesla equivalent magnetic noise magnetoelectric sensor. *The Innovation Materials* **4**:100205.

The ability to detect weak magnetic fields at femtotesla (fT) levels remains a critical obstacle for advancing fields like biomedicine and cross-medium communication. Existing solutions have faced fundamental limitations in operation environments, power efficiency, and sensitivity. Magnetoelectric (ME) sensors offer promising room-temperature alternatives but suffer from intrinsic material noise and extrinsic circuit limitations. Here, we propose a multi-parameter synergistic optimization strategy bridging material design and circuit integration, and establish a theoretical framework for laminated ME composites analysis. Integrated theoretical modeling and experimental validation identify material noise and amplifier noise as dominant noise sources. We go beyond the constraints of material noise and develop multi-longitudinal-transverse (MLT) mode laminates, featuring longitudinally magnetized magnetostrictive layers and transversely polarized piezoelectric fibers connected electrically in series. Compared to LT-mode (longitudinal-transverse) laminates, this design shifts the effective impedance to a reduced equivalent capacitance and increased DC (Direct Current) resistance regime, enabling direct tuning of dielectric loss noise. A single MLT laminates comprising seven LT mode units in a series configuration, achieved an equivalent magnetic noise of 3.84 pT/Hz$^{1/2}$ at 1 Hz. Multiple MLT laminates of parallel array configurations resulted in a threefold reduction in equivalent magnetic noise compared to the series array configuration. Further, by implementing eight MLT units of parallel array configurations, we achieved a record equivalent magnetic noise of 927.8 fT/Hz$^{1/2}$ at 1 Hz—surpassing noise performance of fluxgates and approaching SQUID sensitivity without cryogenic requirements.

INTRODUCTION

Detecting femtotesla (fT)-level magnetic fields under ambient conditions represents a cornerstone technology for bio-magnetic diagnostics and secure cross-medium communication in underwater or subterranean environments.[1-5] Existing solutions, including superconducting quantum interference devices (SQUIDs) and optically pumped magnetometers (OPMs), suffer from stringent operational constraints: cryogenic cooling requirements, bulky infrastructure, limited bandwidth, or excessive power consumption, which hinder their deployment in field systems.[1-3,6] These limitations position ME composites as promising room-temperature alternatives for weak magnetic sensing, leveraging strain-mediated coupling between magnetostrictive and piezoelectric phases to transduce magnetic signals into electrical signals.[7-14] Since layered ME laminates emerged, achieving low-frequency fT detection at ambient conditions has been a central research challenge.[15]

Despite attaining picotesla (pT)-level sensitivity, conventional ME sensors face unresolved trade-offs between interfacial strain coupling efficiency, dielectric dissipation, and amplifier noise floor, precluding operation in the fT regime.[16-20] Overcoming these limitations demands a paradigm shift from isolated material optimization to synergic optimization of sensor systems. Prior efforts have bifurcated into two paths: 1) laminate architecture innovations (e.g., longitudinal-transverse (LT) mode,[21] Metglas/single-crystal hybrids,[22] multi-push-pull mode[23,24]) to enhance ME coefficients and 2) noise suppression techniques (e.g., field modulation,[25-27] differential parallel configurations,[28,29] piezoelectric volume optimiztion[30-34]) to mitigate noise and environmental interference.[35-39] However, these approaches often focus separately on either boosting the responsibility to magnetic signals (α) or mitigating noise, neglecting the critical synergistic optimization of the multi-parameters governing the ultimate sensor performance metric.[23] Therefore, it is imperative to elucidate the coupled mechanisms of material-circuit interactions and establish a framework for multi-parameter synergistic optimization. Although theoretical advances in ME modeling provide foundations for optimizing coefficients and noise,[40-46] early models (e.g., the electromechanical analogy equivalent circuit method[43] and the elastic mechanics mean-field approximation[45]) have oversimplified key physical aspects, impeding accurate prediction of both the enhanced ME coefficients from architectures and integrated sensor systems noise contributions. Thus, a theoretical model for ME coefficients and sensor noise is urgently required to underpin a multi-parameter synergistic optimization strategy.

Here, we present a multi-parameter synergistic optimization strategy that integrates theoretical modeling, material design, and sensor architecture to achieve femtotesla-level magnetic sensing. We first establish the LT-mode theoretical framework, then develop a multi-longitudinal-transverse (MLT) mode laminate featuring series-connected LT units with opposite polarization. This design reduces equivalent capacitance C_E and increases DC resistance R_{dc}, directly suppressing material-derived noise. Further, we demonstrate that series or parallel array of MLT laminates effectively suppress equivalent magnetic noise by precisely balancing sensitivity and noise performance. Through integrated modeling and experiment, we identify that MLT of parallel array configurations achieve threefold lower equivalent magnetic noise compared to series array configurations. By implementing an optimized array of eight MLT laminates in parallel, we achieved a record equivalent magnetic noise of 927.8 fT/Hz$^{1/2}$ at 1 Hz. This work establishes a universal co-design paradigm for ultra-sensitive ME magnetic sensing.

MATERIALS AND METHODS

Materials preparation

The extremely low equivalent magnetic noise ME sensor consists of the PMN-PT single crystal, Metglas2605 (Vacuumschmelze GmbH & Co. KG, Germany). The crystal fibers were fabricated from Mn-doped PMN-PT single crystal boule grown by modified Bridgman technique. The Metglas laminates (140 × 20 × 0.1 mm^3) were fabricated of Metglas ribbons bonded by epoxy resin (West System 105/206): 3 pieces of Metglas were coated with the West System 105/206, then placed in a vacuum bag with negative pressure applied, and cured in an oven at 50°C for 5 hours; excess epoxy on the surface was scraped off with a blade. The crystal fibers with dimensions of 40[001]^L × 2[110]^{W}0.5[110]^T mm^3 (L: length, W: width, T: thickness) were fabricated from as-grown crystal boules after orienting along the [001], [110] and [110] crystallographic direction using an X-ray orientating meter. The fibers were sputtered with gold electrodes using an ion sputtering apparatus (JS1600, SAINTINS) and then polarized under a direct current voltage along the thickness direction. Seven PMN-PT fibers were arranged in opposite polarization directions, and connected in series via electrodes on flexible printed circuit (FPC) with epoxy resin (Emerson Cuming Stycast 1264 A&B). The assembly was placed in a vacuum bag under pressure of around 0.1 MPa, cured in an oven at 50°C for 5 hours. Finally, the two Metglas laminates and one PMN-PT-fibers layer were composited into a sandwich structure using West System 105/206 epoxy resin. After the same curing process as the piezoelectric fibers, the MLT-mode ME laminates was fabricated (Figure S1).

Design of the ME sensor

The ME sensing unit primarily is composed of three core components: (1) MLT-mode ME laminates, (2) neodymium-iron-boron (NdFeB) DC bias magnets, and (3) an encapsulating outer shell. The DC bias magnetic field for the ME composite was provided by a pair of NdFeB magnets, configured to generate uniform magnetic polarization along the longitudinal axis of the piezomagnetic layers. The housing of the ME sensor unit is made of cylindrical engineering plastic. The NdFeB magnets are fixed on the end covers of a cylindrical plastic housing encapsulating the ME sensing unit (Figure S2).

The ME sensor array consists of eight ME sensing units, an operational amplifier circuit, batteries, switches, a protective casing, and an internal chamber for fixing ME sensing units (Figures S3-S4). We tested the variation of the ME coefficients (α_Q) of the sensing units with their spacing, determined the minimum distance between the units, and further designed the fixed inner chamber. The inner chamber can fix at most 8 ME sensing units on the four long axes of the rectangular chamber. Each pair of ME sensing units can be connected in reverse parallel or series to reduce vibration noise. The protective casing and internal chamber of the ME sensor are both fabricated via 3D printing technology (Standard Resin), ensuring mechanical stability and precise dimensional control. The operation amplifier circuit and batteries are housed within the internal chamber, while the switch and signal output BNC (Bayonet Neill–Concelman) interface are positioned on the outer surface of the protective casing for easy operation. The internal chamber was enclosed with a grounded copper foil shield, which effectively mitigates ME interference noise by providing a low-impedance path for stray electromagnetic fields. This grounding strategy enhances the sensor's noise rejection capability, ensuring high-fidelity signal acquisition in low-field environments.

Multi-parameter synergistic optimization

Achieving femtotesla sensitivity requires co-optimizing signal transduction and noise suppression across material and circuit domains. To enable this, we developed a theoretical framework for laminated ME composites. This framework provides a comprehensive description of ME coupling, rigorously accounting for realistic boundary conditions, strain gradients, and dimensional variations across the entire laminate structure—enabling accurate prediction of ME coefficients from quasi-static to resonant frequencies.

Through tensor-level integration of piezoelectric and piezomagnetic constitutive equations into a homogenized mean-field theoretical framework, we establish a refined model that explicitly accounts for interfacial boundary conditions and dimensional asymmetries. It explicitly resolves the full spatial strain distribution (Detailed derivations: Supplementary Information), yielding the frequency-dependent ME voltage field coefficient α_E (Equation 1):

$$\alpha_E = \frac{\overline{E}}{h_1} = \frac{2d_{31}\overline{q}_{11}{}^{p}s_{11}{}^{m}t^{p}v_2 \sin({}^{p}\eta_2)\cdot}{t_2\left[\varepsilon_r\varepsilon_0{}^{p}s_{11}-d_{31}^2\right]\left\{{}^{p}\eta_2{}^{p}s_{11}c_{11}\cos({}^{p}\eta_2)\left(\varepsilon_r\varepsilon_0{}^{p}s_{11}-d_{31}^2\right)+{}^{p}v_2 d_{31}^2\sin({}^{p}\eta_2)\right\}+}, \frac{\cdot\cos({}^{p}\eta_1+{}^{m}\eta)}{+{}^{p}\eta_1{}^{p}s_{11}{}^{m}t^{m}Y^{B}\sin({}^{p}\eta_2)\left[\sin^2({}^{m}\eta)-\cos^2({}^{p}\eta_1)\right]\left\{\sin(2{}^{m}\eta)-\sin(2{}^{p}\eta_1)\right\}} \quad (1)$$

where $\overline{E}$ is the magnitude of the average electric field, h_1 is external alternating magnetic field, d_{31} is the piezoelectric coefficient, $\overline{q}_{11}$ is the piezomagnetic coefficient, ${}^{p}s_{11}$ is the strain tensor component of the piezoelectric phase, ${}^{m}t$ is the thickness of the magnetostrictive phase, t_2 is the thickness of the piezoelectric and magnetostrictive phase in the second composite section, ${}^{p}v_2$ is the volume fractions of the piezoelectric phase in second composite section, ε_r is the permittivity of the piezoelectric phase, and ε_0 is the electrical constant, c_{11} is the effective composite stiffness coefficient of the second composite section, ${}^{m}Y^{B}$ is Young's module of the magnetostrictive phase, ${}^{p}s_{11}$is the volume fractions of the piezoelectric in the second composite section, ${}^{p}\eta_1$ and ${}^{p}\eta_2$ are the phase parameters of the piezoelectric phase in first and second section, ${}^{m}\eta$ is the phase parameter of the piezomagnetic phase. The detailed mathematical derivations for these equations are provided in Supplementary Information. At low frequencies, α_E simplifies to (Equation 2):

$$\alpha_E|_{low-frequency} = \frac{2d_{31}\overline{q}_{11}{}^{p}s_{11}{}^{m}t^{p}v_2}{t_2\left[{}^{p}s_{11}c_{11}\left(\varepsilon_r\varepsilon_0{}^{p}s_{11}-d_{31}^2\right)+{}^{p}v_2 d_{31}^2\right]} \quad (2)$$

Substituting the parameters of ME laminates into the theoretical model yields the frequency-dependent ME field coefficient (Figure 1A).

Then the equivalent magnetic noise can be expressed via the total noise density N_t (including the material noise and circuit noise shown in Supplementary Information) and the sensitivity of ME sensor (Equation 3):

$$\text{Equivalent magnetic noise} = \left.\frac{N_t}{sensitivity}\right| \approx \sqrt{\frac{\frac{4kT}{\omega^2 C_f^2}\times\tan\delta+\frac{1}{\omega^2 C_f^2}\frac{4kT}{R_E}+N_{circuit}}{d_{31}\cdot d_{31}/\varepsilon}} \propto \frac{\tan\delta}{d_{31}g_{31}} \quad (3)$$

Equation 3 shows equivalent magnetic noise scales with $d_{31}\ g_{31}/\tan\ \delta$, which is defined as the Figure of Merit (FOM).[47] To get the highest FOM and the lowest equivalent magnetic noise, we compared the ME coefficients and FOM of PZT-4 ($PbZrTiO_3$), PZT-5, PZT-8, piezoelectric single crystals PMN-PZT ($Pb(Mg_{1/3}Nb_{2/3})O_3$-$PbZrTiO_3$) and PMN-PT ($Pb(Mg_{1/3}Nb_{2/3})O_3$-$PbTiO_3$). We have confirmed that PMN-PT (highest FOM) delivers superior sensitivity and equivalent magnetic noise (Figure 1B).

The performance sensor is determined by both sensitivity and noise characteristics. Using a single LT-mode laminate ME sensor as a reference, the variation of noise components with frequency (Figure 1D) reveals that material-derived noise—comprising DC resistance noise and dielectric loss noise—dominates the total noise floor at 1Hz, followed by feedback resistor noise and operational amplifier current noise. Circuit noise can be mitigated through low-noise operational amplifier selection and optimized circuit design, whereas material noise requires structural engineering at the composite level.

RESULTS AND DISCUSSION

Multi-Longitudinal-Transverse (MLT) mode—units of series configuration

To reduce the material noise, we developed a multi-longitudinal-transverse (MLT) mode comprising multiple piezoelectric fibers polarized along the thickness direction and connected in series, which reduces DC resistance noise and dielectric loss noise by tailoring the material's operational architecture. Figure 2 illustrates the structural design and operational principles of the MLT-mode ME laminates. It adopts a sandwich configuration, featuring of Metglas/Mn-doped $Pb(Mg_{1/3}Nb_{2/3})O_3$-$PbTiO_3$ /Metglas layers (Figure 2A). Each magnetostrictive phase consists of three Metglas alloy (140 mm × 20 mm × 0.015 mm), coupled with resin. The piezoelectric phase consists of seven PMN-PT single crystals (40 mm × 2 mm × 0.5 mm). These piezoelectric units are interconnected electrically in series through a flexible printed circuit (FPC) with interdigital electrodes patterned on a Kapton substrate.

Figures 2B-C illustrate the principle of multi-physical coupling and stress transmission process in ME composites. Figure 2D illustrates the magnetization direction of the magnetostrictive layer and the polarization direction of the piezoelectric fibers. The magnetostrictive layers are magnetized along the longitudinal direction, while the piezoelectric single crystals are polarized alternately in opposite thickness directions. The MLT mode is an evolved architecture based on the LT mode, where the piezoelectric phase comprises several LT-mode piezoelectric single crystals with identical properties. Specifically, the ME charge coefficient scales linearly with the number of units, while equivalent capacitance decreases and DC resistance increases. Crucially, the ME charge coefficient remains unchanged, ensuring that signal sensitivity is maintained while dielectric loss noise and DC leakage noise are directly suppressed according to Equation 3 (The parameters subscripted as LT and MLT are ME composites in LT mode and MLT mode, respectively).

Specifically, as shown in Figures 3A-B, the ME charge coefficient (α_Q) reaches its optimal value of 4500 pC/Oe under the DC bias magnetic field of 9 Oe with the AC driven field of 0.1 Oe at 1 Hz. The extremely high value of α_Q directly determines the signal conversion efficiency of the sensor, thereby leading to sense weak magnetic fields.

Due to the high-impedance characteristics of ME laminates, an impedance-matching operation amplifier becomes imperative. In this work, a charge-mode operation amplifier is employed, with detailed circuit testing provided in the Supplementary Material. The frequency-dependent sensitivity of the ME sensor based on a single MLT-mode ME laminates are shown (Figure 3C). The theoretical lower cut-off frequency of the amplifier is 0.15 Hz. When integrated with a charge-mode amplifier (100 pF), the sensor achieved 21.6 mV/nT sensitivity. Through the equivalent magnetic noise calculation equation, the ME sensor based on a single MLT-mode ME sensor exhibited an equivalent magnetic noise of 3.84 pT/$Hz^{1/2}$ at 1 Hz (Figure S6).

Although the MLT-mode ME sensor achieved significant noise reduction at

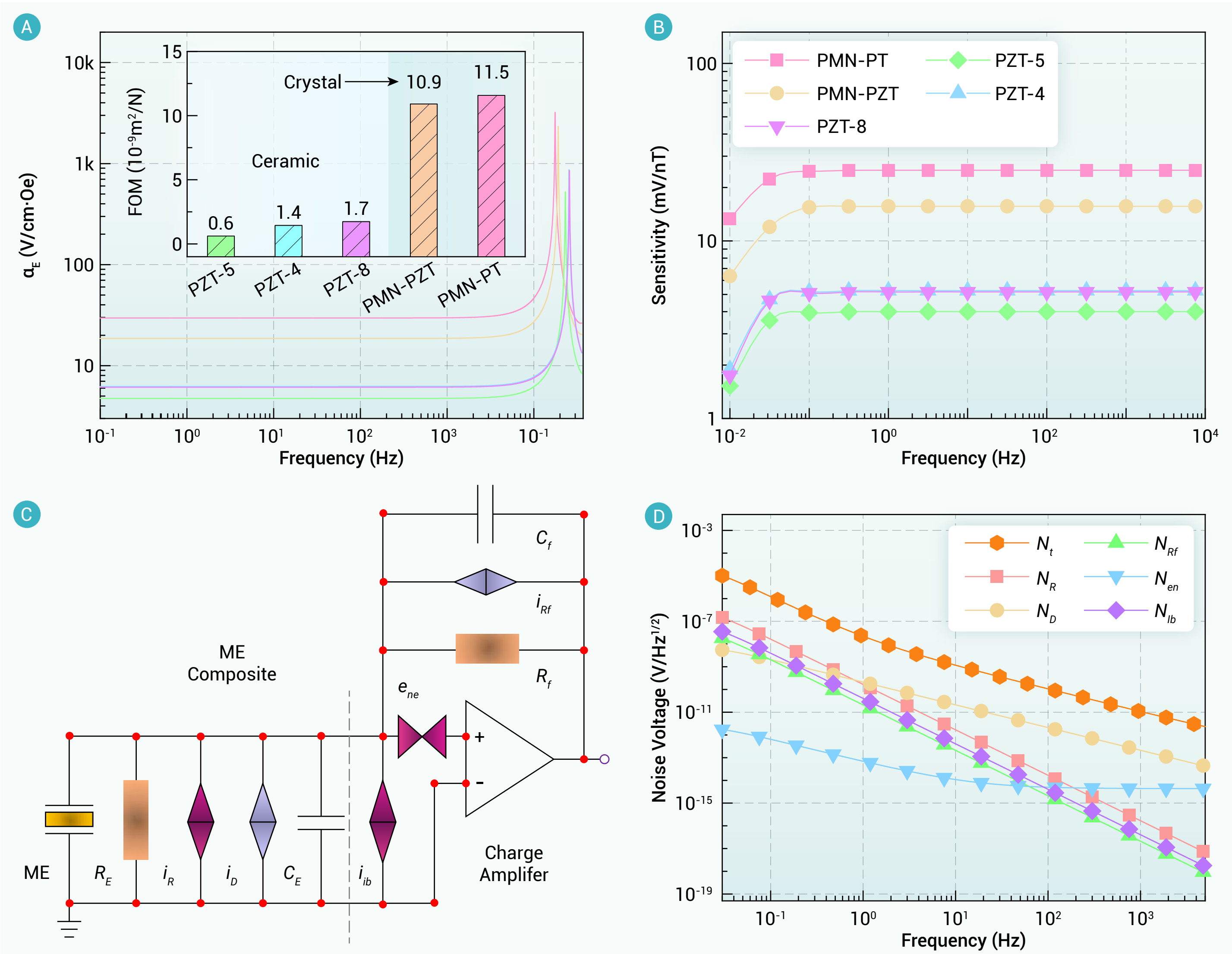

Figure 1. Multi-parameter synergistic optimization and noise characterization of ME sensors (A) Theoretical model simulation of ME coefficient. The inset shows the FOM (figure of merit) of different piezoelectric materials.[47] (B) Simulation of theoretical model for ME sensor response coefficient. (C) Electromechanical analogy equivalent circuit diagram of the ME sensor noise: DC leakage resistance noise (N_R) and dielectric loss noise (N_D) from ME laminates, feedback resistor noise (N_{Rf}), equivalent voltage noise (N_{en}), and current noise (N_{Ib}) from the operational amplifier. (D) Frequency dependence of individual equivalent noise components across a 0.01 Hz to 5 kHz bandwidth.

1 Hz, attaining femtotesla sensitivity requires further optimization beyond the composite level. Crucially, the packaged sensor performance—including circuit integration and environmental stability—becomes critical for practical deployment. Previous theoretical studies have primarily focused on material-level properties, with insufficient attention to optimizing multi-parameters across the material-circuit interface.[25-39] To bridge this gap, we systematically investigate the integration of MLT laminates with a matched amplification circuit. Building on the unit-series architecture of piezoelectric that reduces noise in individual sensing units, we now introduce an array-level strategy where multiple MLT units are interconnected through series/parallel configurations. This approach may represent a fundamental pathway to surmount the sensitivity barrier for femtotesla-level detection Figures S2-S3).

Femtotesla equivalent magnetic noise magnetoelectric sensor——parallel array configuration

To overcome the sensitivity barrier beyond the single MLT-mode ME unit, we systematically optimized ME sensor architecture through array configurations. When ME laminates are integrated with an operation amplifier, the output signal combines responses to target fields and inherent system noise. The equivalent magnetic noise—defined as the noise spectral density referenced to magnetic field input—directly determines the minimum detectable field. Reducing this noise required holistic co-optimization of material properties, circuit parameters, and array topology.

The number of ME units in series is denoted by s, and the number of ME units in parallel is denoted by p. This approach enables systematic optimization of sensor performance by leveraging the scaling laws of series/parallel electrical networks. In the series configuration, the sensitivity of ME sensor remains unchanged as the number of ME laminates in-series increases (Figure 3D). In the parallel configuration, the sensitivity of sensor array increases linearly with the number of ME laminates p. The derived equation for equivalent magnetic noise of series and parallel configuration is as follows (the detailed derivation process can be found in Supplementary Information):

$$\text{Equivalent magnetic noise}|_{Series} = \sqrt{\frac{1}{s}\times\frac{(N_R^2+N_D^2)}{\alpha_Q^2}+\frac{1}{s^2}\times\frac{C_E^2\cdot e_n^2}{\alpha_Q^2}+\frac{C_f^2\cdot e_n^2}{\alpha_Q^2}+\frac{N_f^2+N_{Ib}^2}{\alpha_Q^2}} \tag{4}$$

$$\text{Equivalent magnetic noise}|_{Parallel} = \sqrt{\frac{1}{p}\times\frac{(N_R^2+N_D^2)}{\alpha_Q^2}+\frac{1}{p^2}\times\frac{C_f^2\cdot e_n^2}{\alpha_Q^2}+\frac{C_E^2\cdot e_n^2}{\alpha_Q^2}+\frac{1}{p^2}\times\frac{N_f^2+N_{Ib}^2}{\alpha_Q^2}} \tag{5}$$

To clarify the physical origin of noise suppression differences between

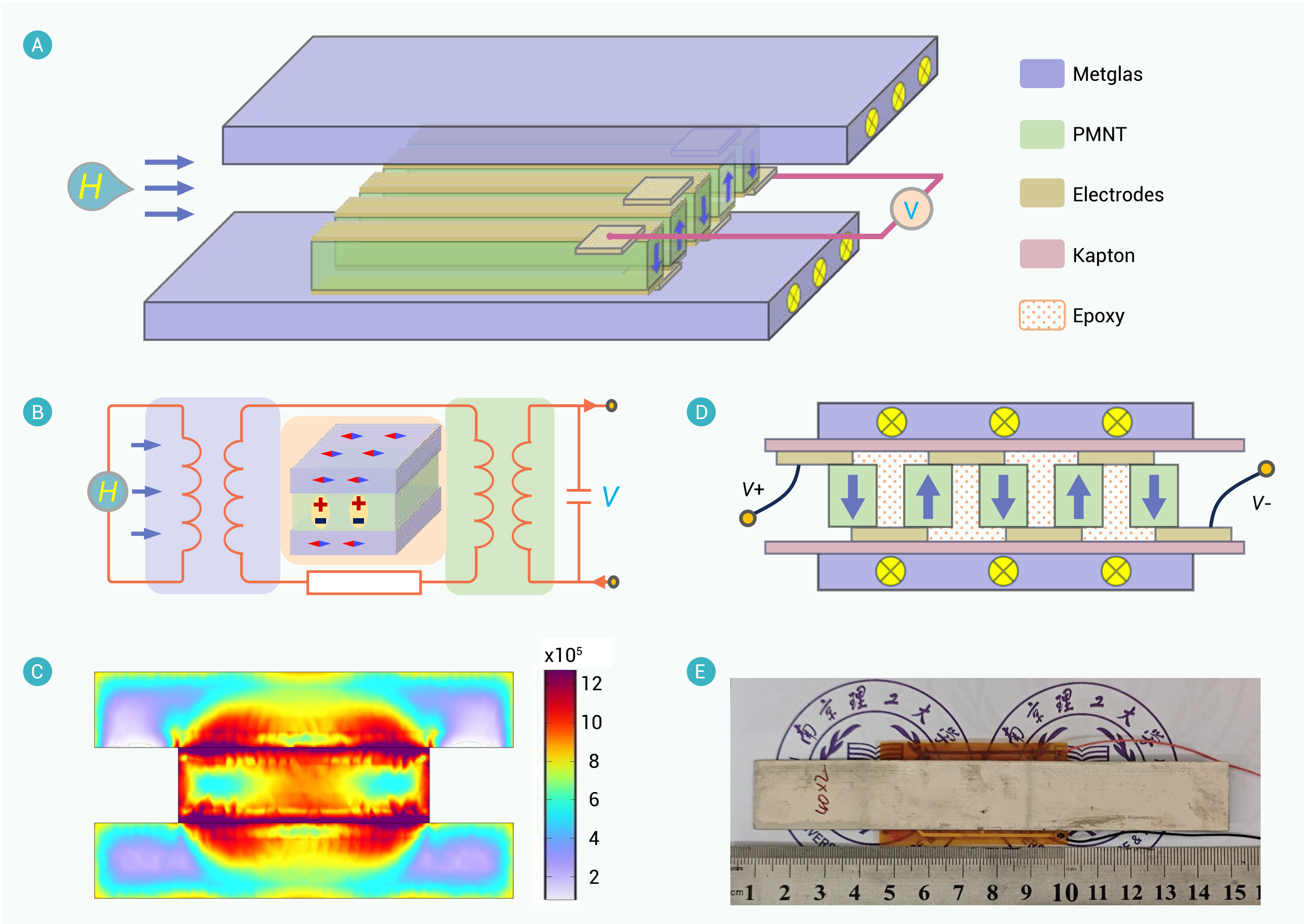

Figure 2. MLT-mode ME laminates and strain-mediated ME coupling principle (A) Schematic architecture of MLT-mode ME laminates: flexible printed circuit board (FPC, Kapton substrate with electrodes), Metglas magnetostrictive layers (FeSiB alloy), and PMN-PT ($Pb(Mg_{1/3}Nb_{2/3})O_3$-$PbTiO_3$) piezoelectric single crystal. (B) Schematic of the strain-mediated ME coupling mechanism. (C) Finite element simulation of strain distribution in MLT-mode. (D) Cross-sectional schematic of MLT-mode ME laminates: Magnetization direction of Metglas (yellow symbols) and polarization direction of PMN-P single crystals (blue arrows). (E) Photograph of the fabricated MLT-mode ME laminates.

series and parallel arrays, we analyze the coupling of charge generation and impedance variation:

In series array configuration, the capacitance C_E of ME units decreased by a factor of $1/s$, but the charge signals of individual units cannot superpose, so α_Q remains unchanged. According to Equations 4-5, the series configuration effectively reduces both DC leakage resistance noise and dielectric loss noise. Although the series configuration has little impact on circuit noise, it moderately suppresses the operational amplifier's equivalent voltage noise. As shown in Figure 4A, simulations indicate that with one to eight ME units in series, the equivalent current noise of the amplifier and the feedback resistor noise remain largely unchanged, while DC leakage resistance noise and dielectric loss noise decrease significantly. Overall, with the increase in the number (s) of serially connected units, the equivalent magnetic noise induced by material noise decreases by a factor of $1/s^{1/2}$.

In the parallel array configuration, the capacitance C_E of ME units increases linearly with the factor of p. Each ME unit generates independent charge signals that superpose linearly with the number of units (p), leading to a proportional increase in α_Q. However, DC leakage resistance noise and dielectric loss noise increase by a factor of $1/p^{1/2}$. Despite the unchanged feedback resistor noise and equivalent current noise of the operational amplifier, the sensitivity of sensor array improves p times, leading to a reduction in equivalent magnetic noise caused by amplifier noise by a factor of $1/p$. Simulation results demonstrated that the parallel configuration significantly reduces equivalent magnetic noise of ME sensors (Figure 4D).

Both series and parallel configurations similarly reduce equivalent magnetic noise caused by material noise to $1/s^{1/2}$ or $1/p^{1/2}$. At low frequencies, the equivalent voltage noise of the operation amplifier has minimal impact on the overall equivalent magnetic noise and can be neglected. For equivalent magnetic noise induced by amplifier noise, the series configuration offers no improvement, while the parallel configuration reduces it significantly by $1/p$. As shown in Figure 4C, the simulated results further confirm the impact of series and parallel configurations on the noise. Estimation indicated that when the ME charge coefficient reached 4500 pC/Oe, 5 units in parallel array configuration can achieve an equivalent magnetic noise of 976.8 fT/Hz$^{1/2}$ at 1 Hz (Figure 4D). In contrast, even with eight laminates components, the equivalent magnetic noise of the series array configuration does not drop below 2.32 pT/Hz$^{1/2}$. Therefore, the parallel configuration demonstrates clear superiority in optimizing equivalent magnetic noise of ME sensors.

We fabricated multiple MLT-mode ME laminates, each individually encapsulated into rod-shaped sensing units. Ferrite magnets provided the DC bias field (9 Oe), ensuring optimal operation. The final sensor housing (Figure S2) comprised a rectangular chamber with eight sensing units fixed to the inner walls.

ME sensing units were connected to the operation amplifier in either series or parallel array configurations. To suppress vibration and acoustic noise, we implemented a differential connection strategy: pairs of units with opposing bias fields and reversed polarities were connected differentially (Figure S3). We systematically tested sensors with 1, 2, 4, 6, and 8 units in series and parallel array configurations, evaluating sensitivity and noise performance

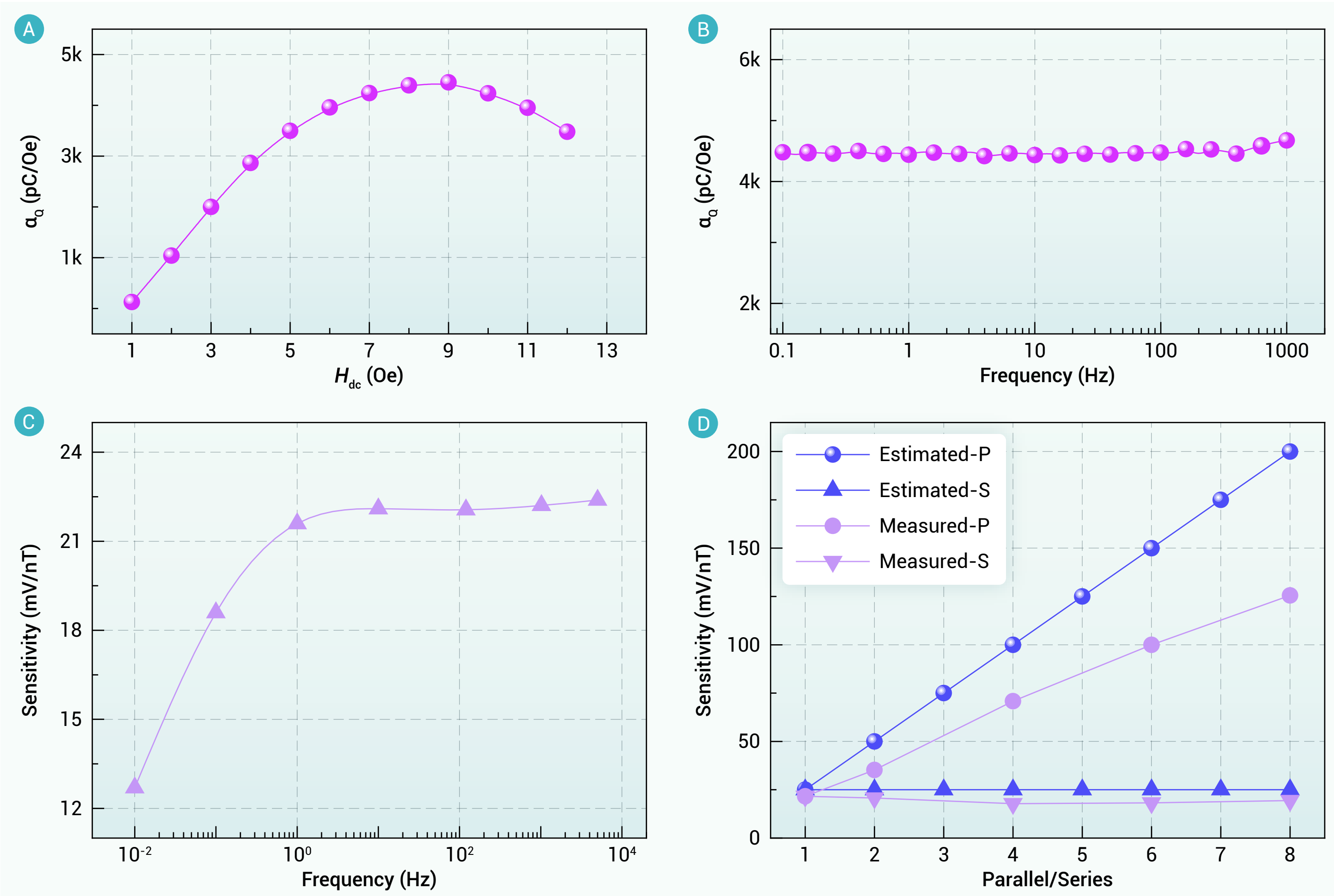

Figure 3. Performance characterization of ME laminates and sensor sensitivity (A) ME charge coefficient (α_Q) of MLT-mode laminates as a function of DC bias magnetic field, exhibiting a peak response at the optimal bias field of 9 Oe. (B) Frequency dependence of α_Q of MLT-mode laminates under optima magnetic bias field. (C) Frequency dependence of sensitivity of ME sensors (ME laminates integrated with a charge amplifier). (D) Sensitivity comparison for parallel (*p*) and series (*s*) configurations: estimated (blue lines) and measured (purple lines) sensitivity as a function of the number of ME units (1-8 units).

(Supplementary Information).

The experimental results demonstrate that in parallel array configuration, the equivalent magnetic noise decreases with an increasing number of ME units, aligning well with theoretical predictions. In contrast, the series configuration exhibits minimal reduction in the equivalent magnetic noise, particularly at low frequencies where practical factors often introduce deviations from ideal scaling. Although the series array reduced equivalent magnetic noise compared to a single unit sensor, it still failed to reach the femtotesla level, demonstrating an equivalent magnetic noise of 2.32 pT/Hz$^{1/2}$ with 8 units. In contrast, the parallel array configuration demonstrated superior noise suppression. While theoretical models predicted that the ME array of 5 MLT units in parallel configuration could achieve 976.8 fT/Hz$^{1/2}$ at 1 Hz. Due to material property variations and residual external noise interference, the experimental setup showed that even the array with 6 parallel ME sensing units in parallel configuration, the femtotesla-level equivalent magnetic noise was not fully realized (1.1 pT/Hz$^{1/2}$). Under optimized conditions, an ME sensor array with eight MLT-mode units in parallel configuration successfully achieved a record equivalent magnetic noise of 927.8 fT/Hz$^{1/2}$ at 1 Hz (Figures 5A-B).

As can be seen in Figure 5C, a systematic comparison of the equivalent magnetic noise at 1 Hz is made between ME sensors[7-9,15-16,19-20,22-24,44] and state-of-the-art magnetometers, including SQUIDs, OPMs, search coils, fluxgates, GMR, Hall, AMR, GMI and TMR sensors.[2-3,9,19] SQUIDs and OPMs can achieve high sensitivity but suffer fundamental limitations: SQUIDs require liquid helium cryostats (bulky systems, high cost), while OPMs have restricted bandwidth (< 100 Hz) and excessive power/volume for applications.[3] As a high-performance active sensor, the fluxgate's power consumption and manufacturing cost further limit its popularization in low-power scenarios. Conventional search coils exhibited intrinsic limitations, including large footprint and elevated low-frequency noise.[19] Despite advantages in miniaturization and moderate power requirements, solid-state sensors (GMR, Hall, AMR, GMI, TMR),[2,3,9] often exhibit equivalent magnetic noise levels higher than 10 pT/Hz$^{1/2}$.

In contrast, the MLT-mode ME sensor array developed in this work achieved equivalent magnetic noise of 927.8 fT/Hz$^{1/2}$ at 1 Hz through simultaneous multi-physics optimization of material parameters and charge amplification circuitry, alongside ultracompact form facto, ultralow power, and low cost. Its performance not only surpasses conventional fluxgate, but also approaches SQUID-level sensitivity without cryogenic infrastructure or high powering. This breakthrough establishes a new "high-sensitivity-low-power-miniaturization" paradigm for weak-field detection.

CONCLUSION

This work breaks the fundamental barrier faced by ME sensors through a tripartite innovation strategy. First, drawing on the piezoelectric and piezomagnetic constitutive equations alongside the mean-field theory, we reconstructed the theoretical model of the ME coefficient for LT-mode ME laminates and subsequently rigorously derived the corresponding theoretical model for MLT-mode ME laminates. We constructed a multi-parameter optimization model that unifies laminate equivalent circuits and amplifier noise mechanisms. Second, the MLT-mode laminates featuring Mn-doped PMN-PT single crystals with alternating thickness-direction polarization enabled reduction of the equivalent capacitance relative to conventional stacked lami-

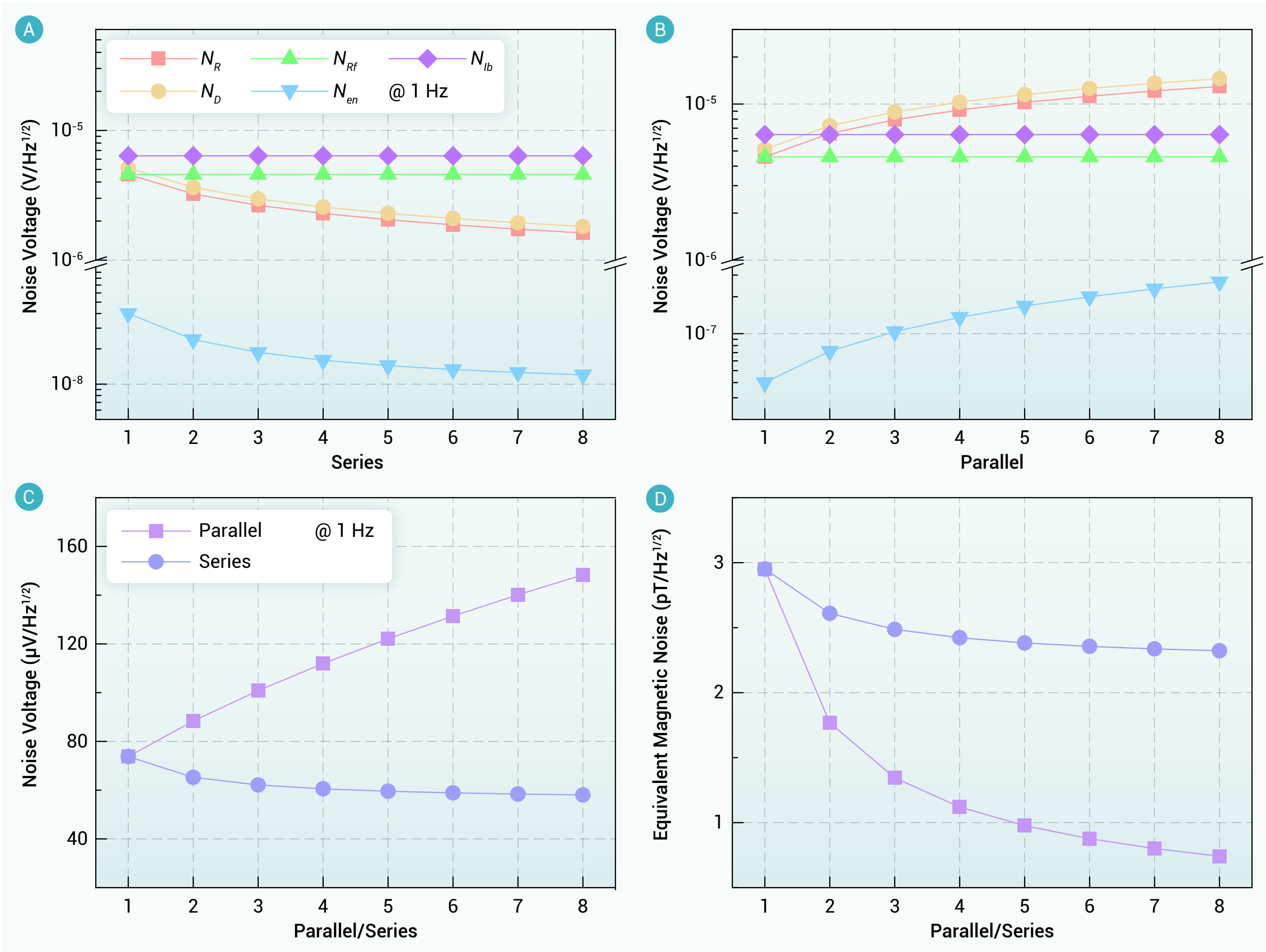

Figure 4. Estimated noise and equivalent magnetic noise of ME sensor array of series or parallel configurations (A) Series array configuration: Noise component variation versus number of ME laminates at 1 Hz. (B) Parallel array configuration: Noise component suppression trend with increasing laminate count. (C) Total noise voltage as a function of the number of ME units in series or parallel array configurations at 1 Hz. (D) Equivalent magnetic noise as a function of the number of ME units in series or parallel array configurations at 1 Hz.

nates, while maintaining a dielectric loss (below 0.01), directly suppressing the noise from the laminates. Third, the design of p MLT ME units in parallel array configurations achieved linear sensitivity enhancement proportional to p. Meanwhile, it reduced equivalent magnetic noise by a factor of $1/p^{1/2}$, outperforming series configurations in noise suppression by a factor of 3.1.

The experimental realization of an ME sensor with eight MLT units parallel array configuration demonstrated an equivalent magnetic noise of 927.8 fT/Hz$^{1/2}$ at 1 Hz—a 75.8% reduction from the single unit. This achievement establishes ME sensors as the first non-cryogenic technology to bridge the "pT-to-fT gap", offering a universal design paradigm for high-sensitivity magnetic detection. Unlike SQUIDs/OPMs, which remain constrained by cryogenics, power, or bandwidth, our approach enables ultracompact, low-power fT sensors. This breakthrough provides a scalable pathway toward compact, low-power sensors for biomagnetic diagnostics and secure cross-medium communication. Future efforts could extend this framework to complex environments or hybrid array architectures, further expanding the operational frontiers of ME technologies.

REFERENCES

1. Pannetier M., Fermon C., Le Goff G., et al. (2004). Femtotesla magnetic field measurement with magnetoresistive sensors. *Science* **304**:1648–1650. DOI:10.1126/science.1096841
2. Khan M. A., Sun J., Li B., et al. (2021). Magnetic sensors-A review and recent technologies. *Eng. Res. Express* **3**:022005. DOI:10.1088/2631-8695/ac0838
3. Dong C., Liang X., Gao J., et al. (2022). Thin film magnetoelectric sensors toward biomagnetism: Materials, devices, and applications. *Adv. Electron. Mater.* **8**:2200013. DOI:10.1002/aelm.202200013
4. Li J., Meng F., Chen S., et al. (2025). Aluminum Scandium Nitride based frequency-switchable acoustic devices for next-generation mobile communication. *Innov. Mater.* **3**:100153. DOI:10.59717/j.xinn-mater.2025.100153
5. Yao Z., Guan Z., Zhang S., et al. (2025). Towards energy-autonomous wearables: Multimodal harvesting technologies and sustainable applications. *Innov. Mater.* **3**:100143. DOI:10.59717/j.xinn-mater.2025.100143
6. Semenok D. V., Troyan I. A., Zhou D., et al. (2025). Observation of the Josephson effect in superhydrides: DC SQUID based on (La,Ce)H_{10+x} with operating temperature of 179 K. *Innov. Mater.* **3**:100115. DOI:10.59717/j.xinn-mater.2024.100115
7. Eerenstein W., Mathur N. D. and Scott J. F. (2006). Multiferroic and magnetoelectric materials. *Nature* **442**:759–765. DOI:10.1038/nature05023
8. Nan C., Bichurin M. I., Dong S., et al. (2008). Multiferroic magnetoelectric composites: Historical perspective, status, and future directions. *J. Appl. Phys.* **103**:031101. DOI:10.1063/1.2836410
9. Ripka P. and Janosek M. (2010). Advances in magnetic field sensors. *IEEE Sens. J.* **10**:1108–1116. DOI:10.1109/jsen.2010.2043429
10. Wu H., Fu S., Wang S., et al. (2022). Electrical current visualization sensor based on magneto-electrochromic effect. *Nano Energy* **98**:107226. DOI:10.1016/j.nanoen.2022.107226
11. Cheng J., Jiao J., Fu S., et al. (2023). Ultra-high baud rate VLF magnetoelectric antenna based on Rosen-type composite. *Appl. Phys. Lett.* **123**:072903. DOI:10.1063/5.0167170
12. Fu S., Cheng J., Jiang T., et al. (2023). Bias-free very low frequency magnetoelectric

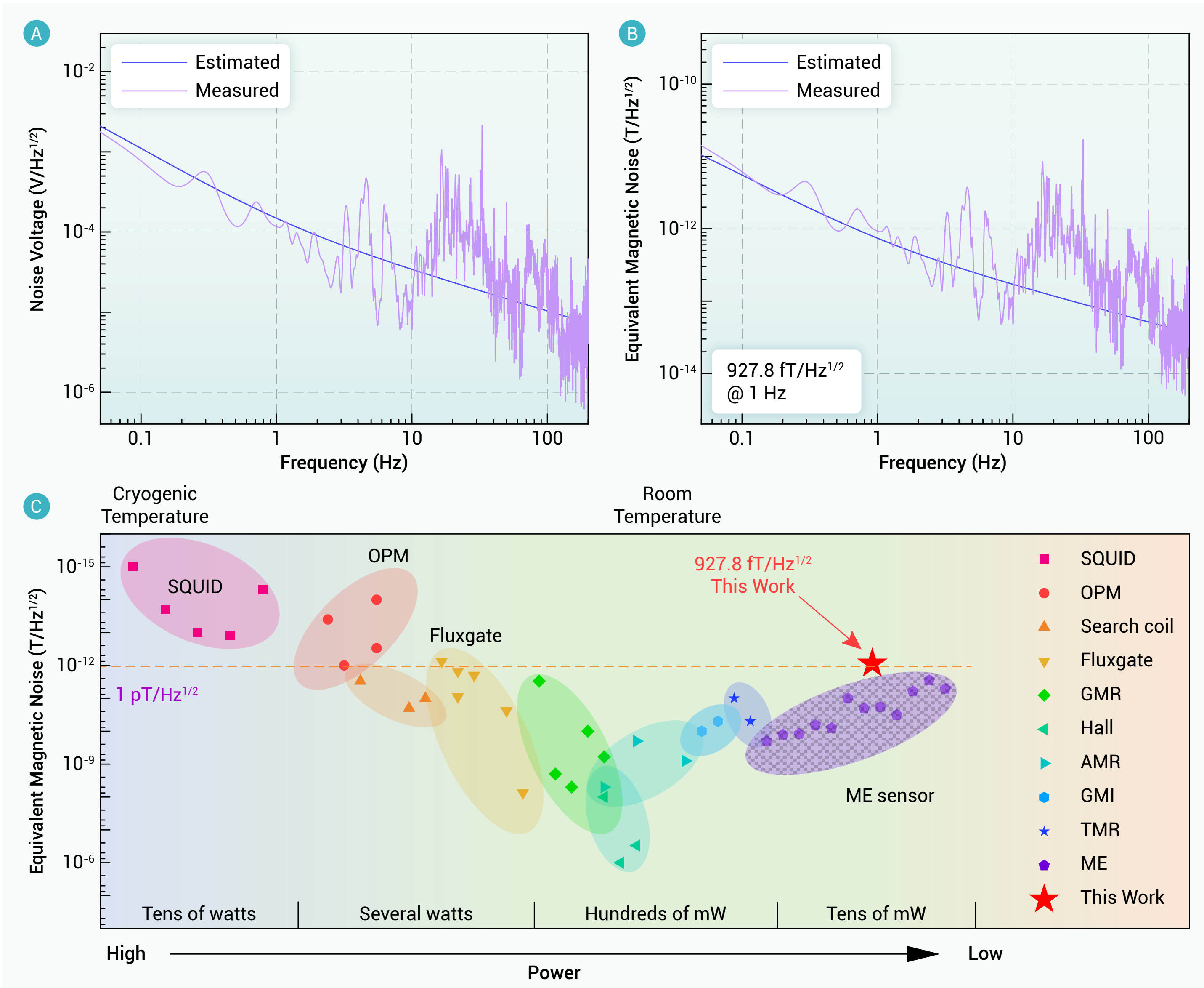

Figure 5. Magnetic noise spectrum, equivalent magnetic field characterization, and performance benchmarking of the magnetic sensor (A) Measured and estimated total noise voltage of the eight-sensor parallel array configuration, including ME laminate noise and amplifier noise components. (B) Measured and estimated equivalent magnetic noise of the 8 units in parallel array configuration. (C) Benchmarking of equivalent magnetic noise against power consumption for state-of-the-art magnetometers: SQUID,[3] OPM,[3] fluxgate,[2,3] search coil,[19] GMR (Giant Magnetoresistance),[2,3,9] Hall (Hall effect sensor),[2,3] AMR (Anisotropic Magnetoresistance),[2,3,9] GMI (Giant Magnetoresistance),[2,3,9] TMR (Tunnel Magnetoresistance),[2,3,9] and ME sensors.[7,9,15,19-20,22-24,44]

antenna. *Appl. Phys. Lett.* **122**:262901. DOI:10.1063/5.0158020
13. Wu H., Jiang T., Liu Z., et al. (2023). Magneto-mechano-electric antenna for portable VLF transmission. *Adv. Electron. Mater.* **9**:2300096. DOI:10.1002/aelm.202300096
14. Fang Z., Jiao J., Wu H., et al. (2025). Crafting very low frequency magnetoelectric antenna via piezoelectric and electromechanical synergic optimization strategy. *J. Materiomics* **11**:100900. DOI:10.1016/j.jmat.2024.05.010
15. Viehland D., Wuttig M., McCord J., et al. (2018). Magnetoelectric magnetic field sensors. *MRS Bull.* **43**:834–840. DOI:10.1557/mrs.2018.261
16. Sreenivasulu G., Laletin U., Petrov V. M., et al. (2012). A permendur-piezoelectric multiferroic composite for low-noise ultrasensitive magnetic field sensors. *Appl. Phys. Lett.* **100**:173506. DOI:10.1063/1.4705305
17. Sreenivasulu G., Qu P., Petrov V., et al. (2016). Sensitivity enhancement in magnetic sensors based on ferroelectric-bimorphs and multiferroic composites. *Sensors* **16**:262. DOI:10.3390/s16020262
18. Turutin A. V., Vidal J. V., Kubasov I. V., et al. (2018). Low-frequency magnetic sensing by magnetoelectric Metglas/bidomain $LiNbO_3$ long bars. *J. Phys. D: Appl. Phys.* **51**:214001. DOI:10.1088/1361-6463/aabda4
19. Thormählen L., Hayes P., Elzenheimer E., et al. (2024). Low-noise inverse magnetoelectric magnetic field sensor. *Appl. Phys. Lett.* **124**:172402. DOI:10.1063/5.0196637
20. Wang Y., Gao J., Li M., et al. (2014). A review on equivalent magnetic noise of magnetoelectric laminate sensors. *Phil. Trans. R. Soc. A.* **372**:20120455. DOI:10.1098/rsta.2012.0455
21. Liu Y., Jiao J., Li L., et al. (2014). Vibrational noise rejection in multilayer structured magnetoelectric sensor. *Sens. Actuators A* **211**:15–18. DOI:10.1016/j.sna.2014.03.002
22. Shen Y., Ma D. and Gao J. (2018). A man-portable magnetoelectric DC magnetic sensor with extremely high sensitivity. *IEEE Electron Device Lett.* **39**:1417–1420. DOI:10.1109/led.2018.2858280
23. Wang Y., Gray D., Berry D., et al. (2011). An extremely low equivalent magnetic noise magnetoelectric sensor. *Adv. Mater.* **23**:4111–4114. DOI:10.1002/adma.201100773
24. Wang Y., Li J. and Viehland D. (2014). Magnetoelectrics for magnetic sensor applications: status, challenges and perspectives. *Mater. Today* **17**:269–275. DOI:10.1016/j.mattod.2014.05.004
25. Petrie J., Viehland D., Gray D., et al. (2011). Enhancing the sensitivity of magnetoelectric sensors by increasing the operating frequency. *J. Appl. Phys.* **110**:124506. DOI:10.1063/1.3668752
26. Petrie J., Gray D., Viehland D., et al. (2012). Shifting the operating frequency of magnetoelectric sensors. *J. Appl. Phys.* **111**:07C714. DOI:10.1063/1.3677840
27. Sun C., Yang W., He Y., et al. (2022). Low-frequency magnetic field detection using magnetoelectric sensor with optimized Metglas layers by frequency modulation. *IEEE Sens. J.* **22**:4028–4035. DOI:10.1109/jsen.2022.3143350
28. Wang Y., Li J. and Viehland D. (2015). A differential magnetoelectric heterostructure: Internal noise reduction and external noise cancellation. *J. Appl. Phys.* **118**:214103.

DOI:10.1063/1.4936263
29. Chu Z., Wang Y., Du Z., et al. (2024). Enhanced detection performance based on a differential ME sensor with strong suppression of vibration interference. *Appl. Phys. Lett.* **125**:182901. DOI:10.1063/5.0232400
30. Fetisov Y. K., Bush A. A., Kamentsev K. E., et al. (2006). Ferrite-piezoelectric multilayers for magnetic field sensors. *IEEE Sens. J.* **6**:935–938. DOI:10.1109/jsen.2006.877989
31. Das J., Gao J., Xing Z., et al. (2009). Enhancement in the field sensitivity of magnetoelectric laminate heterostructures. *Appl. Phys. Lett.* **95**:092501. DOI:10.1063/1.3222914
32. Xing Z., Zhai J., Gao J., et al. (2009). Magnetic-field sensitivity enhancement by magnetoelectric sensor arrays. *IEEE Electron Device Lett.* **30**:445–447. DOI:10.1109/led.2009.2015342
33. Jiao J., Li L., Ren B., et al. (2012). Parallel multilayer magnetoelectric composite based on (1−x)$Pb(Mg_{1/3}Nb_{2/3})$−x$PbTiO_3$ and Terfenol-D coupled with charge mode amplifier. *J. Appl. Phys.* **111**:043909. DOI:10.1063/1.3681818
34. Li M., Gao J., Wang Y., et al. (2012). Enhancement in magnetic field sensitivity and reduction in equivalent magnetic noise by magnetoelectric laminate stacks. *J. Appl. Phys.* **111**:104504. DOI:10.1063/1.4718441
35. Duc N. H. and Giang D. T. H. (2008). Magnetic sensors based on piezoelectric–magnetostrictive composites. *J. Alloys Compd.* **449**:214–218. DOI:10.1016/j.jallcom.2006.01.121
36. Gao J., Hasanyan D., Shen Y., et al. (2012). Giant resonant magnetoelectric effect in bi-layered Metglas/$Pb(Zr,Ti)O_3$ composites. *J. Appl. Phys.* **112**:104101. DOI:10.1063/1.4765724
37. Li L., Jiao J., Chen J., et al. (2013). Magnetoelectric effect of the multi-push-pull mode in 0.35$Pb(In_{1/2}Nb_{1/2})O_3$-0.35$Pb(Mg_{1/3}Nb_{2/3})O_3$-0.30$PbTiO_3$/Metglas magnetoelectric composite. *J. Appl. Phys.* **114**:027011. DOI:10.1063/1.4812221.
38. Ma J., Jiao J., Fang C., et al. (2016). High sensitive nonlinear modulation magnetoelectric magnetic sensors with a magnetostrictive Metglas structure based on bell-shaped geometry. *J. Magn. Magn. Mater.* **405**:225–230. DOI:10.1016/j.jmmm.2015.12.073
39. Chu Z., Dong C., Tu C., et al. (2019). A low-power and high-sensitivity magnetic field sensor based on converse magnetoelectric effect. *Appl. Phys. Lett.* **115**:162901. DOI:10.1063/1.5122774
40. Shen L., Li M., Gao J., et al. (2011). Magnetoelectric nonlinearity in magnetoelectric laminate sensors. *J. Appl. Phys.* **110**:114510. DOI:10.1063/1.3665130
41. Xin Z., Sing M. L. C., Cordier C., et al. (2011). Evaluation of applied axial field modulation technique on ME sensor input equivalent magnetic noise rejection. *IEEE Sens. J.* **11**:2266–2272. DOI:10.1109/jsen.2011.2131647
42. Zhuang X., Lam Chok Sing M., Cordier C., et al. (2011). Analysis of noise in magnetoelectric thin-layer composites used as magnetic sensors. *IEEE Sens. J.* **11**:2183–2188. DOI:10.1109/jsen.2011.2114648
43. Bichurin M. I. and Petrov V. M. (2012). Modeling of magnetoelectric interaction in magnetostrictive-piezoelectric composites. *Adv. Condens. Matter Phys.* **2012**:798310. DOI:10.1155/2012/798310
44. Zhou H., Chen J., Fang Y., et al. (2023). Ultrasensitive modulated magnetoelectric sensors and low-noise readout circuits for DC and very low-frequency weak magnetic signal detection. *IEEE Sens. J.* **23**:13019–13027. DOI:10.1109/jsen.2023.3269437
45. Dong S. and Zhai J. (2008). Equivalent circuit method for static and dynamic analysis of magnetoelectric laminated composites. *Sci. Bull.* **53**:2113–2123. DOI:10.1007/s11434-008-0304-7
46. Fang C., Jiao J., Ma J., et al. (2015). Significant reduction of equivalent magnetic noise by in-plane series connection in magnetoelectric Metglas/Mn-doped $Pb(Mg_{1/3}Nb_{2/3})O_3$-$PbTiO_3$ laminate composites. *J. Phys. D: Appl. Phys.* **48**:465002. DOI:10.1088/0022-3727/48/46/465002
47. Moriana A. D. and Zhang S. (2021). Enhancing electromechanical properties of $Pb(Sc_{1/2}Nb_{1/2})O_3$-$PbZrO_3$-$PbTiO_3$ piezoelectric ceramics via templated grain growth. *Adv. Electron. Mater.* **8**:2100919. DOI:10.1002/aelm.202100919

FUNDING AND ACKNOWLEDGMENTS

This work was supported by the Key Research and Development Program of the Ministry of Science and Technology of China (Grant No. 2024YFB3211800) and the National Natural Science Foundation of China (Grant No. U2441267). The funders had no role in study design, data collection and analysis, decision to publish, or preparation of the manuscript.

AUTHOR CONTRIBUTIONS

Y.J.W. conceived this work and designed the experiments; L.Z.H., J.J., Z.L.Y. and J.J. performed the experiments; the data analysis was performed by L.Z.H. J.J., Z.F. and S.C.H.; L.Z.H., J.J. and Y.J.W. wrote the manuscript. All authors reviewed and commented on the manuscript.

DECLARATION OF INTERESTS

The authors declare no competing interests.

DATA AND CODE AVAILABILITY

Data are available from the corresponding author upon reasonable request.

SUPPLEMENTAL INFORMATION

It can be found online at https://doi.org/10.59717/j.xinn-mater.2026.100205.

LEAD CONTACT WEBSITE

Laboratory of Piezoelectric Materials and Devices: https://piezo.njust.edu.cn/